High-Field de Haas–van Alphen Effect in Rhenium*

A. C. THORSEN, A. S. JOSEPH, AND L. E. VALBY
North American Aviation Science Center, Thousand Oaks, California
(Received 16 May 1966)

The pulsed-magnetic-field technique has been utilized to study the de Haas–van Alphen effect in rhenium. These measurements have indicated the existence of several new segments of Fermi surface in addition to confirming the low-field data reported earlier. The data can be interpreted in terms of a model of the Fermi surface deduced from recent band calculations by Mattheiss.

INTRODUCTION

RECENT measurements of the de Haas–van Alphen (dHvA) effect,[1,2] magnetoresistance,[3,4] and magnetoacoustic absorption[5,6] have provided considerable knowledge of the Fermi surface (FS) of rhenium. The dHvA effect studies, carried out in low magnetic fields, indicated that the FS of this hexagonal close-packed metal consists of at least two closed segments situated somewhere along the A-L symmetry line of the Brillouin zone. Magnetic-breakdown phenomena between the two segments were instrumental in determining their positions in the Brillouin zone, and also their positions with respect to one another. Galvanomagnetic measurements suggest that the FS supports at least two sets of open orbits, one along the $\langle 0001\rangle$ axis, arising from a nearly cylindrical segment and one along the $\langle 10\bar{1}0\rangle$ axis, which results from magnetic breakdown. Magnetoacoustic data have generally been in fair agreement with the FS model deduced from low-field dHvA data, although there is some evidence of other FS segments not observed by the dHvA experiments.

The present study was undertaken in an attempt to map the larger sections of FS. Toward this end, we have utilized the pulsed magnetic-field technique which is particularly suitable for studying short-period dHvA oscillations. The measurements reported herein provide evidence for the existence of several new segments of FS. The data are found to be in good agreement with a theoretical model of the FS of rhenium deduced recently by Mattheiss[7] from a relativistic augmented-plane-wave band calculation.

EXPERIMENTAL

The pulsed-magnetic-field apparatus used in the present study has been described in previous publications.[8] Cylindrical samples of rhenium (diam$\approx$0.030 in., length$\approx$0.15 in.) were spark cut from a single-crystal rod (resistivity ratio$\approx$2700) with the $\langle 0001\rangle$, $\langle 10\bar{1}0\rangle$, and $\langle 11\bar{2}0\rangle$ directions parallel to the axes of the cylinders. Each one was oriented by Laue back-reflection techniques and glued in an appropriate sample holder. When placed in the pickup coil, the samples could be aligned relative to the magnetic field within 1° of the appropriate symmetry axis, and within approximately 3° of the desired symmetry plane. The dHvA oscillations were studied in the $\{0001\}$, $\{10\bar{1}0\}$, and $\{11\bar{2}0\}$ symmetry planes, as well as in portions of a nonsymmetry plane.

MODEL OF THE FERMI SURFACE

A model of the FS of rhenium recently proposed by Mattheiss is found to agree quite well with earlier dHvA-effect and magneto-resistance data. The basic features of the model are illustrated in Figs. 1 and 2. There are three hole surfaces centered around the symmetry point L of the Brillouin zone which are associated with the fifth, sixth, and seventh bands. The smaller of the surfaces (fifth-band holes) are ellipsoidal in shape and correspond to the ellipsoids observed in the earlier dHvA measurements[2] [hereafter referred to as (I)]. The slightly larger sixth-band holes are degenerate with the ellipsoids at a point along the A-L symmetry line and

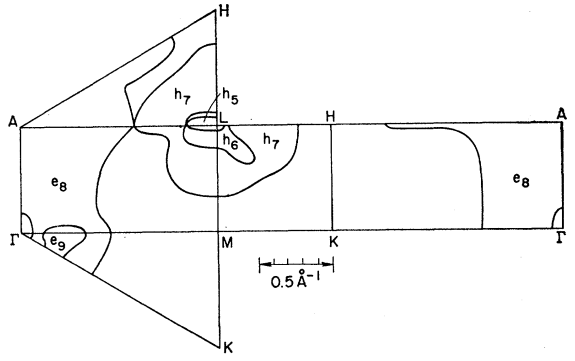

FIG. 1. Intersection of the rhenium Fermi surface with the symmetry planes of the hexagonal Brillouin zone according to the model proposed by Mattheiss. The regions labeled h_5, h_6, and h_7 correspond to holes in the fifth, sixth, and seventh bands, while e_8 and e_9 represent electrons in the eighth and ninth bands.

* Early phases of this study were carried out at the Atomics International Division of North American Aviation Inc. under support by the U. S. Atomic Energy Commission.

[1] A. S. Joseph and A. C. Thorsen, Phys. Rev. **133**, A1546 (1964).
[2] A. S. Joseph and A. C. Thorsen, Phys. Rev. Letters **11**, 67 (1963).
[3] W. A. Reed, E. Fawcett, and R. R. Soden, Phys. Rev. **139**, A1557 (1965).
[4] N. E. Alekseevskii, V. S. Egorov, and B. N. Kazak, Zh. Eksperim. i Teor. Fiz. **44**, 1116 (1963) [English transl.: Soviet Phys.—JETP **17**, 752 (1963)].
[5] C. K. Jones and J. A. Rayne, Phys. Rev. **139**, A1876 (1965).
[6] L. Testardi, Phys. Rev. (to be published).
[7] L. Mattheiss, Phys. Rev. (to be published).
[8] A. C. Thorsen and A. S. Joseph, Phys. Rev. **131**, 2078 (1963), and references therein.

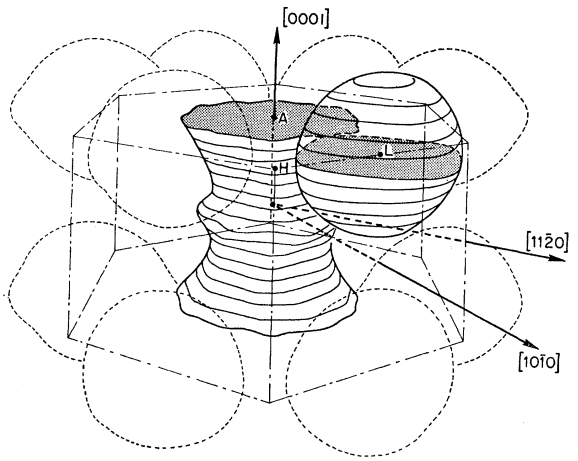

FIG. 2. Three-dimensional model of the seventh-band hole surface and eighth-band electron surface proposed by Mattheiss. The two bands are degenerate at a point along the A-L line.

can be associated with the dumbbell portion of FS deduced in (I). The seventh-band hole surface is a somewhat distorted sphere and has extremal cross sections approximately four times larger than the sixth band holes. Another large segment of FS results from the eighth-band electrons and consists of an undulating cylinder whose axis is along the ΓA symmetry line. This eighth-band-electron surface is degenerate with the seventh-band hole pocket at a point on the AL line. Two other pockets possibly exist according to the model. However, their detailed shapes are very sensitive to the positioning of the Fermi level. One of these, centered at Γ, is almost spherical in shape and can be identified as a section removed from the center of the eighth-band electron cylinder. The other (ninth-band electrons) is possibly a torus-shaped section, again centered around Γ with the axis of the torus along ΓA. For slight changes in the Fermi energy the torus breaks up into six small pockets, each one located on the ΓM line.

RESULTS AND DISCUSSION

The data obtained from the pulsed-magnetic-field study in rhenium can be categorized conveniently in two parts, according to the periods of the oscillations. One group of oscillations has periods ranging from 4×10^{-8} to 16×10^{-8} G^{-1} and was described in some detail in (I). The second group of faster oscillations has periods ranging from 1.0×10^{-8} to 1.7×10^{-8} G^{-1}. In the figures illustrating the period data, we have used solid circles to denote the periods corresponding to the oscillations having the dominant amplitudes. Open circles denote data determined from weak beats in the dominant oscillations. For this reason there is considerably more uncertainty in these points. The data points typically represent an average of several period measurements. The accuracy of the period determinations (solid-circle data) is estimated to be within 3%.

A. Intermediate Periods

The intermediate periods are plotted in Figs. 3–5. We have used Θ to denote the angle measured from the $\langle0001\rangle$ axis in the $\{10\bar{1}0\}$ and $\{11\bar{2}0\}$ planes, and ϕ to denote the angle measured from the $\langle10\bar{1}0\rangle$ axis in the $\{0001\}$ plane. The solid lines are the smoothed steady-field data reported in (I). In most cases the agreement is excellent, although there is some divergence in regions where the amplitudes of the pulsed-field data are weak

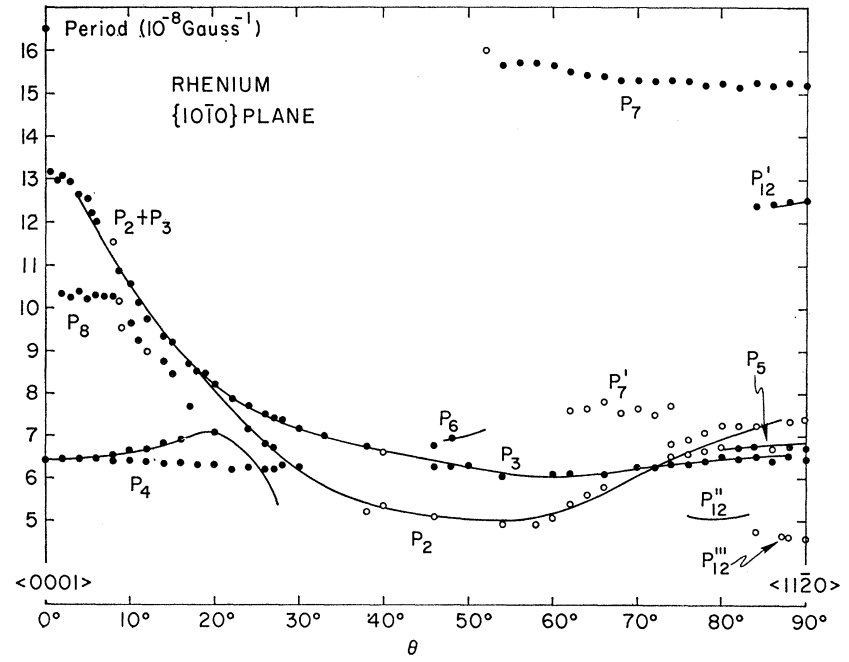

FIG. 3. Intermediate-period data in rhenium in the $\{10\bar{1}0\}$ symmetry plane. The solid lines denote earlier steady-field data. Solid circles denote periods of the dominant oscillations and open circles correspond to periods obtained from weak beats.

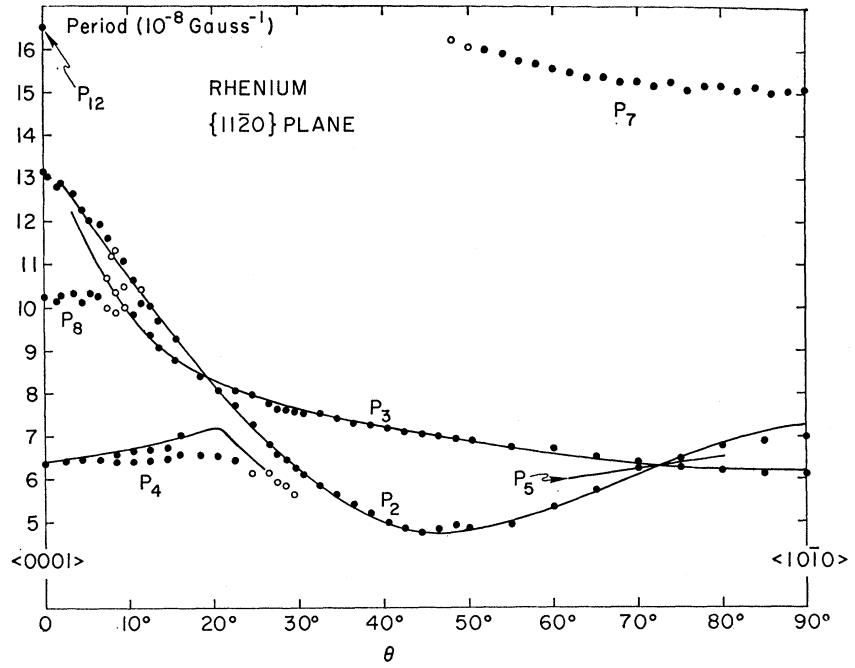

FIG. 4. Intermediate-period data in rhenium in the {11$\bar{2}$0} symmetry plane. The solid lines denote earlier steady-field data. Solid circles denote periods of the dominant oscillations and open circles correspond to periods obtained from weak beats.

and the corresponding errors in the periods are large. It will be noted that several new branches are evident in the pulsed-field data. These branches have constant periods as a function of angle and consequently are not detected by the torque technique. The periods labeled P_2, P_3, and P_4 are associated with the dumbbell segment of FS discussed in (I). The extremal cross sections of this segment may be compared with the sixth-band hole surface predicted by Mattheiss. For the magnetic field parallel to the ⟨0001⟩, ⟨10$\bar{1}$0⟩, and ⟨11$\bar{2}$0⟩ directions, the periods calculated from the model are 14.0, 5.7, and 7.0×10^{-8} G^{-1}, respectively, whereas the experimental values are 13.3, 6.1, and 7.3×10^{-8} G^{-1}. There is one significant difference between the sixth-band hole surface of the Mattheiss model and the dumbbell model[1,2] proposed earlier in that the hole surface has a "dimple" in the ⟨0001⟩ directions. This distortion possibly leads to two extremal orbits when the magnetic field is near the ⟨11$\bar{2}$0⟩ direction and is very likely the origin of P_5. One can interpret P_2 as arising from a central extremal orbit and P_5 from a noncentral extremal orbit.

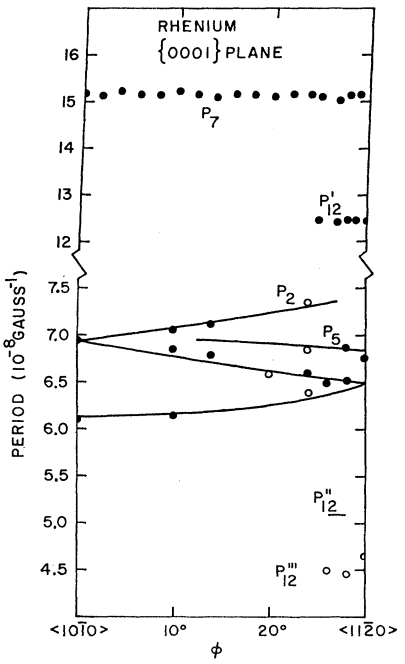

FIG. 5. Intermediate-period data in rhenium in the {0001} symmetry plane. The solid lines denote earlier steady-field data. Solid circles denote periods of the dominant oscillations and open circles correspond to periods obtained from weak beats.

Another period observed near the ⟨11$\bar{2}$0⟩ axis is labeled P_{12}'''. We associate it with a multiple magnetic-breakdown orbit between the dumbbell and ellipsoid. The origin of these weak oscillations is similar to that of the breakdown orbits discussed in (I). The period resulting from such an orbit would be given by $(P_{12}''')^{-1} = (P_2)^{-1} + (P_{12}')^{-1}$. We calculate a value of $P_{12}''' = 4.62 \times 10^{-8}$ G^{-1} from the measured values of P_2 and P_{12}', in excellent agreement with the measured value of 4.6×10^{-8} G^{-1}. It might be pointed out that the period P_{12}''' can be interpreted alternatively as a sum period resulting from the B-H effect[9] since $(P_{12}''')^{-1} \approx (P_3)^{-1} + (P_7)^{-1}$.

In addition to the oscillations related to the dumbbell, two other sets of oscillations with periods in this range of values are found in the pulsed-field measurements. One of these, labeled P_7, is observed to have a constant period of 15.15×10^{-8} G^{-1} throughout the basal plane and is seen to disappear about 40° from the basal plane as the field is rotated toward the ⟨0001⟩ axis. The

[9] D. Shoenberg, Phil. Trans. Roy. Soc. London **A255**, 85 (1962); A. B. Pippard, Proc. Roy. Soc. (London) **A272**, 192 (1963).

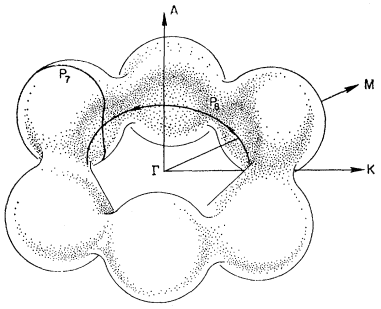

FIG. 6. Model of the ninth-band electron surface proposed by Mattheiss, modified to account for the periods P_7 and P_8.

amplitude of the oscillations decreases gradually as the field is tilted out of the basal plane and the periods exhibit a slight increase in value. The other set of oscillations, labled P_8, is observed near the ⟨0001⟩ axis in both symmetry planes. The oscillations can be followed unambiguously to about 10° from this axis. At this point, P_8 seems to merge with the dumbbell in the $\{11\bar{2}0\}$ plane, and in the $\{10\bar{1}0\}$ plane it appears to decrease rapidly before vanishing. Although the behavior and magnitude of P_8 suggest that it might be associated with another extremal orbit on the dumbbell, any distortion in the dumbbell to produce such an orbit would probably result in *two* additional extremal orbits rather than one. As discussed in the previous section, the band calculations indicate the possible existence of a segment of FS e_9 which is approximately toroidal in shape, and which might be the origin of the periods P_7 and P_8. According to this tentative interpretation, P_8 results from an orbit around the inner diameter of the torus and P_7 arises from an orbit around the body of the torus (see Fig. 6). Since the variation of P_7 with angle suggests a spherical portion of FS, the torus would have to have the approximate shape of six spherical balls connected together to form a ring. Furthermore, the spheres forming the body of the torus must be deformed to have a concave shape on the inner side to explain the constant value of P_8 near the ⟨0001⟩ axis. The approximate shape of such a surface is shown in Fig. 6. No evidence has been found for the orbit around the outside of such a torus or for that around the necks connecting the spherical balls.

The spherical region of such a torus might also be responsible for the long period magnetoacoustic oscillations observed by Jones and Rayne[5] and by Testardi.[6] They find evidence for a spherical segment of surface having a radius of 1.2×10^7 cm^{-1}. If one assumes that P_7 is associated with a spherical surface, the resulting radius would be 1.4×10^7 cm^{-1}, in fair agreement with the magnetoacoustic results.

B. Short Periods

Data on the short-period oscillations observed in the present work are shown in Figs. 7–9. Near the ⟨0001⟩ axis, in both the $\{10\bar{1}0\}$ and $\{11\bar{2}0\}$ symmetry planes, we observe oscillations with very large amplitudes and periods (P_9) which are almost independent of angle. These oscillations, having a period of 1.07×10^{-8} G^{-1}, decrease in amplitude as the field is rotated from the ⟨0001⟩ axis and become vanishingly small approximately 30° from the axis. The origin of P_9 can be attributed to an orbit around the eighth-band electron cylinder centered at Γ. The period predicted by the model is 1.02×10^{-8} G^{-1}, in good agreement with the measured value. The disappearance of P_9 near $\Theta=30°$ is consistent with the model, since the area of the orbit increases rapidly with angle above 30°, leading to a reduction in amplitude. Although one might expect P_9 to exhibit a sharp decrease in value before vanishing, there was no evidence for such behavior.

The shape of the eighth-band electron surface indicates that one should observe another extremal orbit when the field is parallel to the ⟨0001⟩ axis. This orbit is centered at a point approximately one third of the way from Γ to A on the ΓA line. No definite indication of such an orbit has been observed, although one set of oscillations labeled P_{13} in Fig. 7 might be related to this cross section. P_{13}, however, is observed only over a

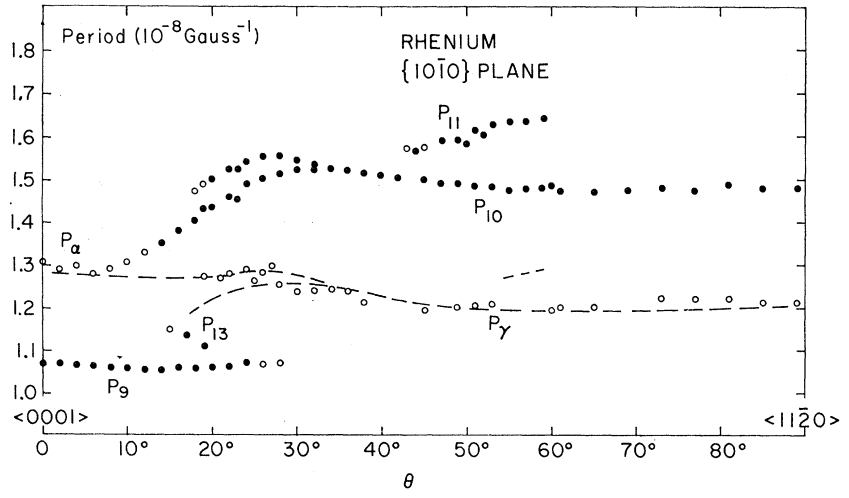

FIG. 7. Short-period data in rhenium in the $\{10\bar{1}0\}$ symmetry plane. The dashed lines represent dHvA periods that might be generated by the *B-H* effect. Solid circles denote periods of the dominant oscillations and open circles correspond to periods obtained from weak beats.

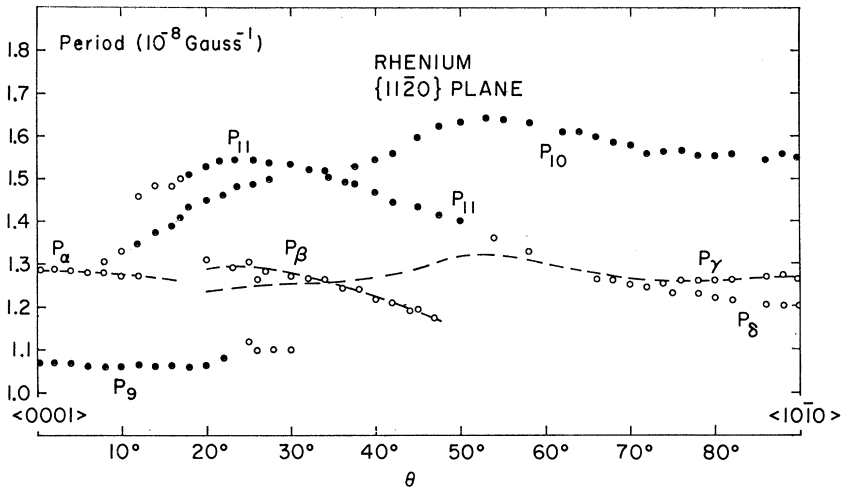

FIG. 8. Short-period data in rhenium in the {11$\bar{2}$0} symmetry plane. The dashed lines represent dHvA periods that might be generated by the *B-H* effect. Solid circles denote periods of the dominant oscillations and open circles correspond to periods obtained from weak beats.

range of approximately 4° in the {10$\bar{1}$0} plane and is not detected in the {11$\bar{2}$0} plane.

In addition, the model predicts extremal orbits centered at the point A on the eighth-band electron cylinder. These orbits would pass through the degeneracy point on the A-L line in the {10$\bar{1}$0} plane and consequently would not be observed. Although one would expect to see oscillations related to such an orbit in the {11$\bar{2}$0} plane, with period values $<10^{-8}$ G^{-1}, no evidence for this orbit has been found.

For $\Theta > 10°$, two other sets of oscillations appear and become stronger in amplitude as Θ increases. The behavior of these periods (labeled P_{10} and P_{11}) is similar in both the {10$\bar{1}$0} and {11$\bar{2}$0} planes, which suggests that both branches are associated with the same segment of FS. In the basal plane (Fig. 9) there appear to be three branches [labeled (1), (2), and (3)] connected with P_{10} and P_{11}, although they cannot be followed unambiguously through 90°. From the apparent connectivity in the basal plane we deduce that the surface giving rise to these oscillations must have 180° symmetry.

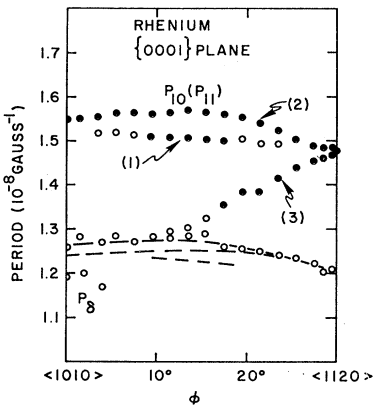

FIG. 9. Short-period data in rhenium in the {0001} symmetry plane. The dashed lines represent dHvA periods that might be generated by the *B-H* effect. An additional period of 3.34×10^{-9} G^{-1} is found near the ⟨11$\bar{2}$0⟩ axis (not shown), resulting from a giant orbit discussed in text. Solid circles denote periods of the dominant oscillations and open circles correspond to periods obtained from weak beats.

In terms of the FS model, the seventh-band hole surface satisfies the symmetry requirements and is the right size to explain the periods P_{10} and P_{11}. This hole surface is centered on the symmetry point L and bulges out in the ⟨10$\bar{1}$0⟩ directions where it touches the eighth-band electron surface at one point on the A-L line. This degeneracy would lead to a disappearance of extremal orbits around the surface for certain directions of the magnetic field. In particular, for $\Theta \approx 0°$, extremal orbits would pass near or through the degeneracy point leading to a disappearance of the associated dHvA oscillations. This could account for the apparent vanishing of P_{10} and P_{11} for Θ near 0°. Similarly, for the field in the (10$\bar{1}$0) plane, central extremal orbits on two of the seventh-band hole surfaces (located along the [10$\bar{1}$0] and [$\bar{1}$010] axes) would pass through the degeneracy point. One would therefore expect to see only one branch in the period curves in this plane. The fact that two branches are observed over some regions of the {10$\bar{1}$0} plane suggests that the second branch (labeled P_{11} in Fig. 7) is a result of noncentral extremal orbits on the seventh-band hole surface.

It is apparent from the data in the basal plane (Fig. 9) that as the field is rotated away from the ⟨11$\bar{2}$0⟩ axis, the period $P_{10}(P_{11})$ is approximately constant for 30° [branch (1)], increases slightly but remains essentially constant for the next 30° [branch (2)], and finally decreases after 60° [branch (3)]. Midway between the ⟨10$\bar{1}$0⟩ and ⟨11$\bar{2}$0⟩ axes, the oscillations related to the lower branch (3) become weak in amplitude. Similarly, in the {11$\bar{2}$0} plane the oscillations related to the lower branch (labeled P_{11} in Fig. 8) become vanishingly small $\approx 30°$ from the ⟨10$\bar{1}$0⟩ axis. According to the model the two branches should join along the ⟨10$\bar{1}$0⟩ direction at a period value of $\approx 1.1\times10^{-8}$ G^{-1}. We therefore assume that the weak oscillations P_δ are related to this surface, and join with $P_{10}(P_{11})$. One possible explanation for the

drastic reduction in amplitude around the $\langle 10\bar{1}0\rangle$ axis is that the spin-splitting factor[10] $\cos(\pi m^* g/2m_0)$ goes to zero.

The size of the seventh-band hole surface is found in general to be in good agreement with experiment. For the particular segment located along the $[10\bar{1}0]$ axis, the model predicts the following periods (in units of 10^{-8} G^{-1}): $P=1.47$ for $\mathbf{H}\|[\bar{1}2\bar{1}0]$; $P=1.44$ for $\mathbf{H}\|[01\bar{1}0]$; $P=1.37$ for $\mathbf{H}\|[11\bar{2}0]$; and $P=1.1$ for $\mathbf{H}\|[10\bar{1}0]$. These are to be compared with the values 1.48 (extrapolated), 1.55, 1.48, and 1.2±0.1 (extrapolated), respectively. The first of the values ($\mathbf{H}\|[\bar{1}2\bar{1}0]$) is an extrapolated value because branch (1) of the data in Fig. 9 cannot be followed all the way into the axis. According to the model, this branch should disappear near the $\langle 11\bar{2}0\rangle$ axis where the orbits are approaching the degeneracy point on the A-L line.

The data in Fig. 10 are obtained in a nonsymmetry plane which contains the $\langle 0001\rangle$ axis but is tilted 5° from the $\langle 11\bar{2}0\rangle$ axis (see insert in Fig. 10). The middle branch of the data can be followed to approximately 25° from the basal plane before the amplitude becomes vanishingly small. The orbits corresponding to this branch are observed near the basal plane because they do not intersect the A-L line, but as the sample is rotated toward the $\langle 0001\rangle$ axis, the orbits get closer to the degeneracy point with a consequent reduction in the amplitude of the oscillations.

We have not yet discussed the various other periods that are evident in Figs. 7–9, viz., those labeled as P_α, P_β, P_γ. The oscillations corresponding to these periods are in general weak in amplitude and usually appear as weak beats in the dominant oscillations. Estimates of the sum and difference periods that could be generated

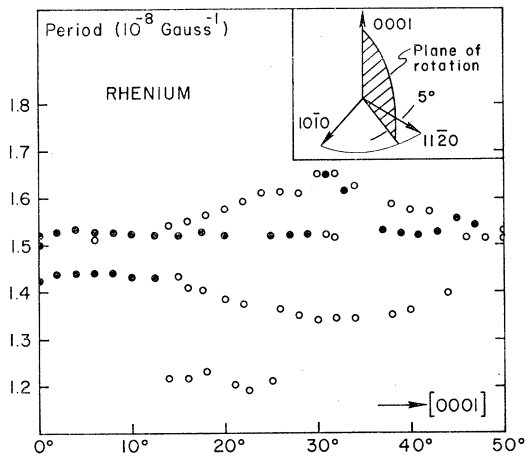

FIG. 10. Short-period data in rhenium in a plane shown in the inset. Solid circles denote periods of the dominant oscillations and open circles correspond to periods obtained from weak beats. The abscissa angle is measured from the basal plane.

[10] A. S. Joseph and A. C. Thorsen, Phys. Rev. **134**, 979 (1964), and references therein.

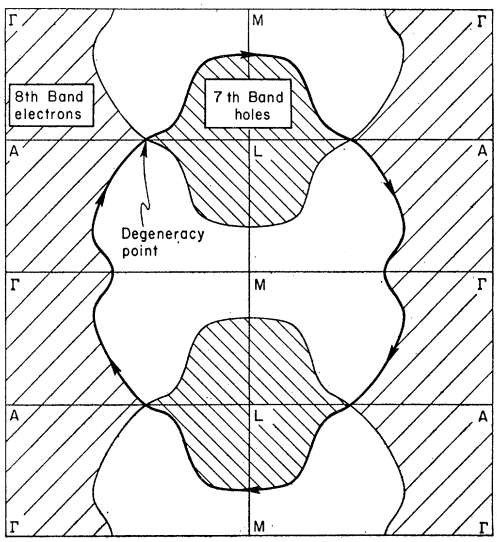

FIG. 11. Cross section of the Fermi surface in the ΓALM plane showing the seventh-band hole and eighth-band electron surfaces and illustrating the origin of the giant orbit discussed in text. The heavy solid line denotes the orbit with $\mathbf{H}\|\{11\bar{2}0\}$.

by the B-H effect[9] show good agreement with the periods associated with these weak oscillations. Accordingly, we have plotted with dashed lines in Figs. 7–9 the sum or difference periods between the dominant oscillations associated with the dumbbell and the dominant oscillations of the periods in the $1.0-1.7\times10^{-8}$ G^{-1} range. The excellent agreement with the experimental points leads us to make this tentative assignment, although we have no other direct experimental evidence to substantiate this interpretation.

Additional short-period oscillations are observed when the magnetic field is near the $\langle 11\bar{2}0\rangle$ axis. These fast oscillations can be detected within 2° of the $\langle 11\bar{2}0\rangle$ axis in the basal plane and to almost 5° from the axis in the $\{10\bar{1}0\}$ plane in fields $\approx$ 140 kG. The period value is 3.34×10^{-9} G^{-1} and appears to be constant over the angular range of observation. According to the FS model, this short period can be interpreted as arising from a giant orbit between the eighth-band electron surface and the seventh-band hole surface. The path of this orbit in the $\{10\bar{1}0\}$ plane is indicated in Fig. 11. The period value calculated from the model is 3.4×10^{-9} G^{-1}, in excellent agreement with experiment. The observation of this large orbit constitutes one of the most conclusive pieces of evidence for the validity of the proposed FS model.

CONCLUSIONS

This pulsed-field dHvA effect study has revealed the existence of several new segments of FS in addition to confirming the low-field data reported earlier. The data can be interpreted in terms of a model of the FS deduced from recent band calculations by Mattheiss.[7] In most cases the agreement between theory and experiment is quite good. The fifth- and sixth-band holes

of the model adequately explain most of the long-period data (P_1,P_2,P_3,P_4,P_5) and agree with the model proposed in (I). The seventh-band hole surface appears to account very nicely for the majority of the data (P_{10}, P_{11}, and P_δ) taken at high fields. The eighth-band electron surface predicts three extremal cross sections for the magnetic field near the ⟨0001⟩ axis, but only one of these (P_9) has been definitely observed in the present study. The reason the other orbits are not observed (except perhaps P_{13}) is not presently understood. However, the band calculations as well as the magnetoresistance data indicate a very low mobility for this band, which could make these orbits difficult to detect. A toroidal-shaped segment of surface corresponding to a ninth-band electron surface possibly accounts for two new periods (P_7,P_8) observed in the pulsed-field experiments. The model predicts several other extremal orbits on the ninth-band electron surface that have thus far not been detected. The rather weak oscillations with periods denoted by P_α, P_β, and P_γ are tentatively attributed to *B-H* effects in the magnetization. The most conclusive evidence supporting the validity of the model is provided by the breakdown orbit between the eighth-band electron and seventh-band hole surfaces.

ACKNOWLEDGMENTS

The authors wish to thank H. Nadler for growing the high-purity rhenium crystal used in this study and D. Swarthout for orienting the samples. We are indebted to L. Mattheiss for supplying Figs. 1 and 2 and for communicating the results of his calculations prior to publication. We have benefited from a number of fruitful discussions with L. Testardi and acknowledge a critical reading of this manuscript by T. G. Berlincourt.

PHYSICAL REVIEW VOLUME 150, NUMBER 2 14 OCTOBER 1966

Linear-Response Theory of the Electron Mobility in Molecular Crystals*

P. GOSAR† AND SANG-IL CHOI
University of North Carolina at Chapel Hill, Chapel Hill, North Carolina
(Received 8 February 1966; revised manuscript received 9 June 1966)

The effect of the fluctuations of the polarization energy and the transfer integrals on the excess electron and hole motion in aromatic crystals, in particular anthracene, has been studied. The Kubo linear-response theory and the Wannier representation have been used. At temperatures higher than the Debye temperature, the electron-phonon interaction through the fluctuation of polarization energy is found to be considerably greater than that due to the transfer-integral fluctuation for anthracene crystal. A high-temperature formula for the mobility tensor has been derived, which may be considered as a generalization of the random-walk diffusion-model formula. This mobility expression consists of two parts, representing tunneling with and without phonon assistance. The temperature dependence due to electron-phonon interaction comes in through the thermal-equilibrium occupation number of phonon modes, $n(\lambda)$, and well-defined quantities $\alpha(i,j)$. Fairly good agreement between the calculated and measured values of mobility has been obtained.

I. INTRODUCTION

IN this paper we consider the effect of the fluctuations of the polarization energy and the transfer integrals on the electron and hole motion in aromatic solids. The excess electron is not screened in molecular crystals and therefore it produces a strong polarization of the surrounding molecules. The electronic polarization energy of the lattice by the excess charge is about -1.74 and -1.28 eV[1] for anthracene and naphthalene, respectively. The acoustic and other intermolecular vibrations of the lattice displace or change the orientation of the molecules in the crystal. This produces the fluctuations of the polarization energy and thus couples the electron with phonons. Another relaxation mechanism is due to the fluctuations of the transfer integrals. These integrals depend strongly on the intermolecular distances and are therefore affected by the lattice waves. This type of interaction was studied by Glarum[2] and extensively in a recent paper by Friedman.[3] The above-mentioned relaxation mechanisms are probably the strongest ones in molecular crystals.

In order to calculate the mobility we use the linear-response theory initiated by Kubo and Tomita.[4,5] Further, all calculations are performed by using the Wannier representation[6] for charge carriers.

* Supported by the Advanced Research Projects Agency.
† On leave of absence from Nuklearni Institut "J. Stefan," Lujbljana, Yugoslavia.
[1] L. E. Lyons and J. C. MacKee, Proc. Chem. Soc. **1962**, 71 (1962).
[2] S. Glarum, J. Phys. Chem. Solids **24**, 1577 (1963).
[3] L. Friedman, Phys. Rev. **140**, A1649 (1965).
[4] R. Kubo and K. Tomita, J. Phys. Soc. Japan **9**, 888 (1954).
[5] R. Kubo, J. Phys. Soc. Japan **12**, 570 (1957).
[6] G. H. Wannier, Phys. Rev. **52**, 191 (1937).